Opacity of Dense, Cold, and Strongly Coupled Plasmas

A. N. Mostovych, L. Y. Chan, and K. J. Kearney
Laser Plasma Branch, Plasma Physics Division, U.S. Naval Research Laboratory, Washington, D.C. 20375

D. Garren,[1] C. A. Iglesias,[2] M. Klapisch,[3] and F. J. Rogers[2]
[1]*Science Applications International Corporation, McLean, Virginia 22102*
[2]*Lawrence Livermore National Laboratory, P.O. Box 808, Livermore, California 94550*
[3]*ARTEP, Inc., Columbia, Maryland 20899*
(Received 22 March 1995)

The physics of dense [$(1-5) \times 10^{19}$ cm^{-3}], cold (1–15 eV), strongly coupled ($\Gamma \sim 0.7$) plasmas is probed with 0.351, 0.527, and 1.054 μm opacity measurements in well characterized, laser-heated, aluminum plasmas. Current opacity models are tested, for the first time, in the regime where the probing photon energies are of the same order as the average interparticle interaction energies in the plasma. Predicted enhancements of the opacity at low temperatures are not observed, but overall agreement between experiment and theory is within a factor of 2.

PACS numbers: 52.25.Qt, 52.25.Rv, 52.50.Jm

At low temperatures, the electrons and ions of dense plasmas interact strongly to produce highly nonideal gas systems. The interaction to thermal energy ratio Γ is no longer small as in "weakly coupled" ideal gas plasmas. The opacity of strongly coupled plasmas (SCP) is of fundamental interest because it is sensitive to nonideal effects through its strong dependence on the equation of state, particle collisions, plasma microfields, and atomic line shapes in the plasma. The largest nonideal effects are expected for photons with energies comparable to the plasma interaction energies, i.e., $h\nu/kT \leq \Gamma$. At these energies the photon-plasma interaction is primarily determined by electron-ion collisions and transitions between high-lying atomic levels which are subject to strong perturbations from the plasma. The opacity and transport properties of dense plasmas are important issues in astrophysics, laser-fusion, and shock wave research, as well as in the physics of high current discharges. The physics of SCP's [1] and the opacity [2] of dense plasmas have been the subject of vigorous theoretical and numerical investigations with relatively few experiments. Comparisons between opacity models show reasonable agreement between models for high temperature plasmas with high-charge-state ions, but rather poor agreement for low temperature plasmas with low-charge-state ions [3]. Recently, the hot, high-charge-state plasma regime has been investigated by several soft x-ray and XUV opacity experiments [4]. Previous opacity work with low temperature plasmas was primarily with plasma arcs [5], shock waves in high density gases [6], or laser vaporization and heating of thin metal films [7]. Typically, the arc plasma experiments were at low densities such that $\Gamma < 0.2$, whereas in the shock wave experiments the opacity was not measured directly but was inferred from plasma emission measurements. In our early work [7] with laser-heated vapors, the plasma expansion from laser heating was only measured in two dimensions (2D), making computer modeling of the plasma hydrodynamics necessary to fully analyze the data. In this letter, we report on new multi-wavelength opacity experiments with laser-heated metallic vapors. New diagnostics and instrumentation measure the plasma expansion in 3D, removing previous uncertainties. The UV to IR emission spectrum and the 0.351, 0.527, and 1.054 μm opacity of strongly coupled plasmas for $n_e \approx (1-5) \times 10^{19}$ cm^{-3}, $T_e \approx 1-15$ eV, and $\Gamma = 0.3-0.8$ are measured under controlled and well diagnosed conditions. Comparisons with calculations show agreement, within a factor of 2, with the STA [8] and OPAL [9] opacity models.

Similar to Ref. [7], a laser-produced plasma is used as the source for these experiments; see Fig. 1. A glass substrate is coated with an Al film, and a laser beam vapor-

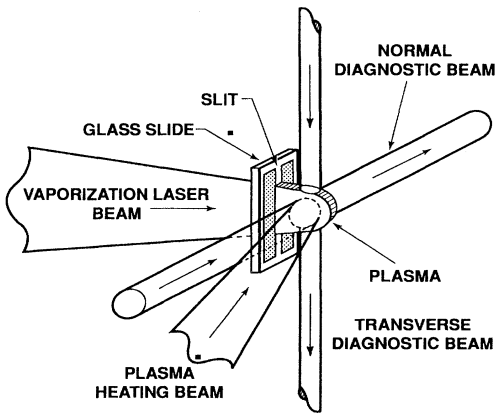

FIG. 1. Schematic of experimental setup. A laser vaporizes a thin aluminum film from a glass substrate. The aluminum vapor flows through a thin slit (100 μm) and is heated and ionized by a second laser. Multiwavelength probes measure the plasma absorption coefficient while transverse interferometer beams measure the plasma density profile.

 0031-9007/95/75(8)/1530(4)$06.00

izes this film by irradiation through the glass. The expanding supersonic vapor, with a diameter comparable to the laser focal spot ($d \sim 1.0$ mm), flows through a slit ($\Delta x \approx 100$ μm) which limits its transverse extent and total mass. After the vapor slab has reached the appropriate expansion length ($l \approx 1000$ μm at $t \approx 100$ ns) and desired vapor density, a second laser ($\lambda = 1.054$ μm, $10^{10}-10^{11}$ W/cm^2) is used to ionize the Al vapor. The heating occurs over a time of about 5–8 ns and produces a fully ionized plasma (roughly 1000 μm by 1000 μm) with an average ionization $\langle Z \rangle \approx 1-4$. Three short pulse (700 ps) probe beams (1.054, 0.527, and 0.351 μm) measure the transmission through the plasma, normal to the slab geometry. The beams are focused to a small spot ($d \approx 100$ μm) in the center of the plasma to provide spatial resolution and to ensure a uniform density in the focal plane. The degree of transmission is measured with a set of fast ($\tau \approx 350$ ps) incident and transmitted photodiodes. The transmission probes are much brighter than the plasma, and the transmission measurements are not affected by plasma emission. Two unfocused interferometry beams, one normal and one transverse, measure the line integrated density from the two orthogonal orientations. These measurements are unfolded to give the density profile along the line of sight of the transmission measurement. The emission of the plasma, in the focal volume of the transmission probes, is measured with an absolutely calibrated 0.5 m monochromator with a temporal resolution of 0.5 ns. The plasma temperature is determined from the absolute emission and the degree of transmission at 0.527 μm. For plasmas in local thermodynamic equilibrium (LTE), these quantities are related to the average temperature through the radiation transfer equation and Kirchhoff's law [10], i.e., $I(\nu, \Gamma) = I_p(\nu, \Gamma)(1 - I/I_0)$, where $I_p(\nu, \Gamma)$ is the Planck distribution, I/I_0 is the transmission fraction, and ν is the frequency of the absorbing radiation. The plasma emission spectra (2000–8000 Å) are recorded with a 0.33 m spectrometer coupled to a streak camera or gated microchannel plate detector.

The initial plasma geometry is slablike; however, the density profile of the plasma along the transmission-probe line of sight evolves into a Gaussian-like profile as a result of heating and expansion; see inset in Fig. 2. The profiles are symmetric as long as the vapor areal-mass-density remains below some critical value. In these experiments, the maximum Al mass density is restricted (to approximately 4.5×10^{-4} g/cm^3, $N_{\text{ion}} \sim 10^{19}$ cm^{-3}) to ensure symmetry in the density profile and to ensure full fringe visibility in the highly absorbed transverse interferometer beam. The average mass density (i.e., ion density) is inferred from the measured electron density and temperature and the degree of ionization given by a Saha equation calculation for Al. The Saha equation and the equations of state in the OPAL and STA codes give ion densities which are within 2%–3%. Typical electron densities in the experiment, averaged over the line-of-sight profile, are plotted in the solid circles of Fig. 2. The uncertainty in the temperature for these data is typically 10%–20%. The solid curve through the data is a Saha calculation for an average mass density of 3.6×10^{-4} g/cm^3. The spread in the data is due to shot-to-shot variations in the mass density of the aluminum vapor, resulting from variations in the film thickness, laser power, beam alignments, and slit width. The solid triangles in Fig. 2 correspond to the strength of the ion coupling parameter [$\Gamma = e^2 Z^{5/3}(4\pi N_e/3)^{1/3}/T_e$]. Coupling between ions is the strongest ($\Gamma \approx 0.75$) at temperatures (4–5 eV), where the population of triply ionized aluminum peaks. For the most part the plasmas are in LTE, with collisional excitation and relaxation rates dominating over radiative rates [11]. However, for Al IV, the rate of collisional excitation between the ground and 1st excited states (excitation time $\approx$ 10 ns at 10 eV) is too slow to bring the excited and higher ionization states above the Al IV ground state into LTE in the 5–8 ns heating time of the experiment. As a result, for temperatures in the 10–15 eV range, where there is significant excitation and ionization of Al IV, the degree of ionization may not reach its LTE value. The worst case deviation from LTE is estimated from a Saha calculation (dashed curve in Fig. 2) for which all states above the Al IV ground state are assigned a statistical weight of zero.

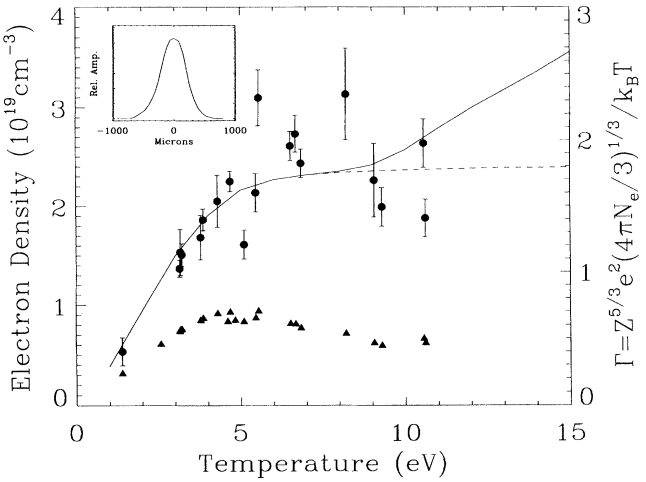

FIG. 2. Measured electron densities as a function of plasma temperature. Solid curve due to Saha equation calculation for an aluminum mass density of $\rho_m = 3.6 \times 10^{-4}$ g/cm^3. Dashed curve estimates the worst case deviation from LTE. Triangular data points correspond to the strength of the ion coupling parameter. Curve in inset is a typical transverse density profile of the plasma.

Opacity measurements are taken in the region where deviations from LTE are small. The transmission of the laser probes (1.054, 0.527, and 0.351 μm) is measured at the peak of the heating pulse and in tempo-

ral and spatial synchronization with the interferometry and absolute emission measurements. The transmission T through the plasma is related to the absorption coefficient κ by $T = \exp[-\int \kappa(x)dx]$. For comparison between experiment and theory it is convenient to define an average absorption coefficient $\langle\kappa\rangle = -\ln(T)/L$, where L is an average plasma thickness calculated from the measured density profile $n_e(x)$ such that $L\int n_e^2(x)dx = \{\int n_e(x)dx\}^2$. With this choice, processes which depend on $n_e(x)^2$ are well described by average quantities even though the plasma profile is not flat. This model is useful for our conditions because the STA and OPAL opacity codes and the data show a $n_e(x)^2$ dependence for the absorption coefficient. In practice, L is also used to calculate the average electron densities. L is comparable to the thickness containing 90% of the plasma mass (0.06–0.1 cm) and is about 1.5 times the full width at half maximum (FWHM) of the density profile.

The 0.351, 0.527, and 1.054 μm absorption coefficients are plotted in Fig. 3. These opacity data are a subset corresponding to only those measurements having an initial mass density of $\rho_0 = (3.6 \pm 1.8) \times 10^{-4}$ g/cm^3. In addition, the data are scaled by $(\rho_0/\rho_m)^2$ to account for the finite distribution of actual mass densities ρ_m and the n^2 dependence of the opacity. Error in the data is minimized by averaging over multiple data in temperature steps of 0.5 eV. The error bars include instrumental, alignment,

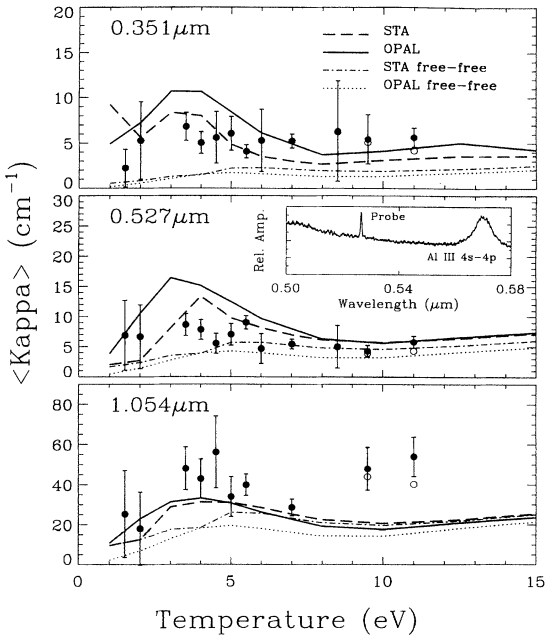

FIG. 3. The measured absorption coefficient at 0.351, 0.527, and 1.054 μm compared to OPAL and STA model calculations for an aluminum mass density of $\rho_m = 3.6 \times 10^{-4}$ g/cm^3. Open circles indicate impact of possible non-LTE density distribution on the opacity. Inset contains typical ($T \sim 5$ eV) spectra in the vicinity of the 0.527 μm probe.

and calibration uncertainties of the transmission measurements, as well as the effects of the uncertainties in density and temperature on the absorption coefficient. The effect of non-LTE density distributions on the opacity is to reduce the absorption coefficient around 10 eV, as indicated by the open data points.

To better characterize the conditions under which the opacity was measured, simultaneous time-resolved emission spectra were recorded in the 0.25–0.70 μm range. Detectors sensitive in the 1 μm range were not available for this experiment. The 0.351 and 0.527 μm probing wavelengths are in smooth regions of the emission spectra between very broad emission lines; see inset in Fig. 3. The spectra also revealed some narrow but very strong resonance absorption lines (transitions from the ground state) originating from neutral aluminum and from neutral slit material impurities. These features are far from the probing wavelengths and are the result of emission from the plasma interior being absorbed in the low-density wings of the plasma profile. Here, the temperature is sufficiently low ($\approx$1 eV) to permit finite populations of ground-state neutral atoms, and the lines are not strongly broadened by high density. The population of impurities is estimated from the relative strength of the impurity-to-aluminum lines and is found to be less than 1% of the aluminum population. At this concentration, even in the plasma interior, changes in the opacity from impurities are not expected at wavelengths outside the narrow resonance lines.

The data are compared to predictions of the STA and OPAL opacity models. They calculate the complete absorption coefficient $\kappa = \kappa_{ff} + \sum\kappa_{bf} + \sum\kappa_{bb}$, including free-free, bound-free, and bound-bound contributions. These are LTE models that include contributions from all ionization stages in the plasma, as well as from all LTE populated bound and free states of each ionization stage. In the STA model the large number of bound states that are populated in LTE are grouped into smaller supertransition arrays of similar energy-level configurations. The energy, strength, and variance of transitions between arrays are determined from solutions of the Dirac equation in parametric potentials, self-consistently optimized for each super configuration. Energies and strengths are corrected to first order to account for departure from pure jj coupling. The population of levels follows Fermi statistics; dense plasma effects are incorporated with an ion-sphere radius model of ionization potential lowering and by including degeneracy effects for the continuum. The OPAL model uses parametric potentials, but it differs in that all terms are accounted for in detail, and LS coupling determines the configuration term structure. In OPAL, dense plasma effects are included in the equation of state and in the occupation number of bound states through systematic expansions of the grand canonical partition function for a system of electrons and nuclei interacting in a Coulomb potential. In both models, bound transition energies do not have spectroscopic accuracy ($\Delta E \approx 1\%$), and pertur-

bation of states by the plasma microfields is taken into account with a semiempirical and semiclassical electron-impact broadening theory [12]. Free-free transition cross sections for the two models are calculated from their respective plasma-screened parametric potentials with quantum mechanical partial-wave expansions. These models have been successful in reproducing previous x-ray ultraviolet opacity measurements in higher temperature experiments [4] but have not been tested in the low-temperature UV-visible-IR region. This low-temperature, low-photon-energy regime is different because free-free transitions now form a significant fraction of the opacity, the broadening of bound transitions by plasma perturbations is greater than configuration splitting, and many of the contributing bound transitions are near the plasma-perturbed continuum edge.

Initial comparisons of the models to the data differed by factors of 2 to 5. Spontaneous emission reductions to the opacity had to be included (STA), and approximate free-free calculations had to be replaced with full dipole matrix evaluations (STA and OPAL). In Fig. 3, the OPAL and STA calculations are displayed alongside the data. The calculations are based on the average density and temperature measured in the experiment. In practice, the plasmas have finite density and temperature gradients. The sensitivity of the calculations to these gradients was checked by integrating the local OPAL opacities over the measured electron-density profile and several physically reasonable temperature profiles. The set of temperature profiles was chosen to span the range from the ideal, flat profile, to the worst-case, highly peaked profile. The temperature profiles are constrained by the measured density profile, via the equation of state, and by the requirement to reproduce the measured plasma emission. The difference in opacity between calculations using average values vs full profile averages increases as the temperature profile is peaked, limiting to about 15%–20% for the worst case where the concomitant mass density, as dictated by the equation of state, becomes flat. The actual deviation will be less than 20% because an expanding plasma can not have a flat mass-density profile.

Both STA and OPAL predict enhancement of bound state contributions in the 2–6 eV temperature range, where the Al III ionization state and its large set of spectral lines in the UV-visible-IR range are well populated. Even though the probing wavelengths do not coincide with aluminum absorption lines, the wings of many spectral lines contribute to the absorption as a result of spectral line broadening by the dense plasma. The measured opacity, while greater than the free-free opacity, is nearly constant and does not show significant enhancement in this temperature range. The 0.351 and 0.527 μm data indicate that bound states contribute less than is calculated by STA and OPAL. The sensitivity of the opacity to line broadening issues is illustrated by the difference in STA and OPAL opacities. The OPAL bound state contributions are larger, primarily as a result of broader (2×) line profiles in OPAL calculations. The role of spectral line broadening is being investigated in a new set of experiments and will be published elsewhere. The overall differences between experiment and theory imply theoretical uncertainties on the order of 20%–50% in this dense, low temperature regime.

The opacity (0.351, 0.527, and 1.054 μm) of dense, cold, and strongly coupled plasmas ($\Gamma \approx 0.5-0.7$) has been measured under well characterized conditions. Comparison of the data with current opacity codes such as OPAL and STA show that both bound-bound and free-free absorption processes are important in this parameter regime, but that their relative contributions are not yet certain. Overall agreement between experiment and theory is within a factor of 2.

The NRL authors were supported by the U.S. Office of Naval Research.

[1] Good reviews are found in S. Ichimaru, H. Iyetomi, and S. Tanaka, Phys. Rep. **149**, 91 (1987); S. Ichimaru, *Statistical Plasma Physics* (Addison-Wesley, Reading, MA, 1992); *Strongly Coupled Plasma Physics,* edited by H. M. Van Horn and S. Ichimaru (University of Rochester, Rochester, 1993), and references within.

[2] See, for example, *Radiative Properties of Hot Dense Matter,* edited by W. Goldstein, C. Hooper, J. Gauthier, J. Seely, and R. Lee (World Scientific, Singapore, 1991).

[3] S. J. Rose, J. Quant. Spectrosc. Radiat. Transfer **51**, 317 (1994).

[4] P. T. Springer *et al.,* Phys. Rev. Lett. **69**, 3735 (1992); L. B. da Silva *et al.,* Phys. Rev. Lett. **69**, 438 (1992); J. M. Foster *et al.,* Phys. Rev. Lett. **67**, 3255 (1991); T. S. Perry *et al.,* Phys. Rev. Lett. **67**, 3784 (1991).

[5] V. E. Gavrilov *et al.,* Sov. J. Opt. Technol. **49**, 403 (1982); M. M. Popović, and D. S. Dordević, in *Strongly Coupled Plasma Physics,* edited by H. M. Van Horn and S. Ichimaru (University of Rochester, Rochester, 1993).

[6] V. E. Bespalov, V. K. Gryaznov, and V. E. Fortov, Sov. Phys. JETP **49**, 71 (1979); D. Erskine, B. Rozsnyai, and M. Ross, J. Quant. Spectrosc. Radiat. Transfer **51**, 97 (1994).

[7] A. N. Mostovych *et al.,* Phys. Rev. Lett. **66**, 612 (1991).

[8] A. Bar-Shalom *et al.,* Phys. Rev. A **40**, 3183 (1989).

[9] F. J. Rogers and C. A. Iglesias, Astrophys. J. Suppl. Ser. **79**, 507 (1992).

[10] Ya. B. Zel'dovich and Yu. P. Raizer, *Physics of Shock Waves and High-Temperature Hydrodynamic Phenomena* (Academic Press, New York, 1966).

[11] H. R. Griem, *Plasma Spectroscopy* (McGraw-Hill, New York, 1964).

[12] M. S. Dimitrijevic and N. Konjevic, J. Quant. Spectrosc. Radiat. Transfer **29**, 451 (1980).